Chinese Chemical Letters 35 (2024) 109189

Contents lists available at ScienceDirect

Chinese Chemical Letters

journal homepage: www.elsevier.com/locate/cclet

A new metal–organic rotaxane framework for enhanced ion conductivity of solid-state electrolyte in lithium-metal batteries

Ying Li[b], Yanjun Xu[b], Xingqi Han[a,*], Di Han[b], Xuesong Wu[b,*], Xinlong Wang[a,b], Zhongmin Su[a,b,c,*]

[a] School of Marine Science and Engineering, Hainan Provincial Key Lab of Fine Chemistry, School of Chemical Engineering and Technology, Hainan University, Haikou 570228, China
[b] School of Chemistry and Environmental Engineering, Changchun University of Science and Technology, Jilin Provincial Science and Technology Innovation Center of Optical Materials and Chemistry; Jilin Provincial International Joint Research Center of Photo-functional Materials and Chemistry, Changchun 130022, China
[c] State Key Laboratory of Supramolecular Structure and Materials, Institute of Theoretical Chemistry, College of Chemistry, Jilin University, Changchun 130021, China

ARTICLE INFO

Article history:
Received 9 July 2023
Revised 23 September 2023
Accepted 9 October 2023
Available online 10 October 2023

Keywords:
Cucurbit[6]urils
Metal–organic rotaxane frameworks
Ionic conduction
Solid-state electrolyte
Lithium-metal batteries

ABSTRACT

The composite polymer electrolyte has been obtained *via* incorporating **LiCUST-701** (a new metal–organic rotaxane framework modified by Li^+) into poly(ethylene oxide) (PEO) matrix and give a high ionic conductivity of 4.02×10^{-4} S/cm at 60 °C. DFT calculations were used to visualize the possible diffusion pathway of Li^+. The all-solid-state cell assembled with $LiFePO_4$, composite polymer electrolyte and lithium metal foil delivered with excellent cycling capability and stability even under high current densities.

Lithium metal batteries using lithium metal as an anode material have attracted much attention from researchers due to their high specific capacity and energy density. The accidental hazards of lithium metal batteries caused by volatile and flammable liquid electrolytes have been a major concern in the study of lithium metal batteries [1–3]. As compared with traditional liquid electrolyte, emerging solid-state electrolyte (SSE) has the characteristics of high safety, stability and mechanical strength. Thus, the SSE can not only ensure the safety of lithium metal battery, but also improve its performance [4–7]. Besides, the SSE possesses the advantages of good compatibility with lithium metal cathode and inhibition of lithium dendrite generation [3,8–10]. However, the practical application of all-solid-state lithium-metal batteries is severely hampered by the lower Li-ion conductivity and too small lithium mobility number of SSEs. Therefore, it is a significant and challenging task to design and synthetize novel SSE materials with high ion conductivity and large lithium migration number.

Of all the present solid electrolyte materials, inorganic solid electrolytes and polymer electrolytes are more widely studied. Inorganic SSEs usually exhibit relatively high conductivity, but their brittleness and hardness also lead to the increase of interfacial resistance with electrodes [2,3]. In contrast, polymers as electrolytes have some unique advantages. The good interfacial contact with electrode of polymer electrolytes results in a lower interfacial impedance between the electrolytes and the electrode. In particular, polymer electrolytes based on poly(ethylene oxide) (PEO) with high polarity and pliability are regarded as good polymer electrolyte matrix materials [2,11–13]. However, However, PEO-based solid electrolyte systems usually exhibit relatively low ion conductivity at ambient temperature. When operated at high temperatures above 80 °C, it may undergo the degradation of mechanical properties and limitation of the electrochemical stability window. Moreover, the growth of lithium dendrites reduces the safety performance of solid-state polymer electrolyte systems [14–16]. Recently, various methods, such as the addition of plasticizers or inorganic solid nanoparticles have been adopted to improve the low electrical conductivity and poor mechanical strength of PEO-based polymer [17–20]. In addition, metal-organic frameworks (MOFs) have attracted much attention in the field of solid-state electrolytes and other energy fields because of their unique structure and properties [21–23]. The ordered structure of MOFs and abundant pore channels might provide conduction paths for Li^+. Metal–organic

* Corresponding authors.
E-mail addresses: hanxq@hainanu.edu.cn (X. Han), wxs@cust.edu.cn (X. Wu), zmsu@nenu.edu.cn (Z. Su).

https://doi.org/10.1016/j.cclet.2023.109189
1001-8417/

rotaxane frameworks (MORFs) are a special class of MOFs where pseudorotaxanes are used as organic ligands. In general, pseudorotaxanes contain two parts. Part of it is axial molecule, and the other part is macrocyclic molecule. The axial molecule be used to connect metal nodes while, macrocyclic molecule can be used as functional sites. CB[6] molecules as macrocyclic components has been widely used for assembling pseudorotaxanes, which are like pumpkin rings with open ports at both ends. The negative electric carbonyl functional groups distributed in port part of CB[6], and the positive electric methylene and hypomethyl groups exist on the outer wall of CB[6], which can produce ion-dipole interaction with inorganic anions and can be conducive to construct functional pseudorotaxane ligands. The functional groups or active sites in the framework are likely to interact with lithium salts and contribute to efficient Li^+ conduction in the channels [21,24]. In addition, the nano-scale MOFs in composite polymer electrolyte, which act as solid fillers can effectively improve the mechanical strength of polymer electrolytes to a certain extent, then can guide the uniform deposition of Li^+ at the interface, and reduce the generation of lithium dendrites [25–28].

In this work, a new metal-organic rotaxane framework (MORF) named CUST-701 (CUST = Changchun University of Science and Technology) has been successfully synthesized under hydrothermal conditions. Then, the CUST-701 is modified *via* ion-exchange method to obtain LiCUST-701. The composite polymer electrolyte is constructed *via* incorporating LiCUST-701 into PEO polymer matrix. DFT theoretical calculations were used to visualize lithium-ion transport pathway involving transfer between sulfonic acid groups in MORF. Experimental results indicate that the composite electrolyte materials prepared with LiCUST-701 as fillers and PEO polymers, can effectively promote the transport of Li^+ through electrostatic interaction forces with the active sites in the MORFs, which guides the uniform deposition of Li^+ and inhibit the growth of lithium dendrites. The cyclic stability of all-solid-state cell assembled with composite polymer electrolyte, $LiFePO_4$ as cathode and lithium metal foil as anode showed a capacity of 148 mAh/g at the first discharge and 134 mAh/g after 100 cycles, with a capacity retention rate of 90.5%.

$[Zn(PR43)(H_2stp)_2(H_2O)_2]\cdot 3.5H_2O$ (CUST-701) has been synthesized *via* reaction of cucurbit[6]uril (CB[6])-based pseudorotaxane ([PR43], Fig. 1a), H_2stp and Zn^{2+} on hydrothermal condition, and its exact structure was obtained by X-ray single-crystal diffraction, and corresponding crystal data are shown in Tables S1 and S2 (Supporting information). The CUST-701 crystallizes in monoclinic system with the $P2_1/C$ space group. The metal centre of CUST-701 is six-coordination pattern including two pyridine N atoms from different [PR43]s connector (Zn–N: 2.125(3)–2.152(3) Å), two oxygen atoms from the separated carboxylic acid group of 2-H_2stp in a bidentate mode, and two oxygen atoms from two coordinated water molecules (Zn–O: 2.075(2)–2.305(2) Å), which forms a one-dimensional sawtooth chain structure through the linkage of pseudorotaxanes ligands (Fig. 1b and Figs. S2–S4 in Supporting information).

The phase purity of the crystalline material was verified by PXRD and FT-IR (Figs. S5 and S6 in Supporting information). TGA shows that the CUST-701 had excellent thermal stability and could maintain framework integrity up to 365 °C (Fig. S7 in Supporting information). Optical microscopy images of CUST-701 are shown in Fig. S8 (Supporting information). Transparent long blocky crystals can be observed. SEM images and corresponding elemental mapping of CUST-701 are shown in Fig. S9 (Supporting information). SEM and corresponding elemental distribution analysis of ion-exchanged CUST-701 were performed. As shown in Fig. S10 (Supporting information), individual elements including fluorine were uniformly distributed on LiCUST-701, this indicates the successful introduction of lithium ions into MORFs. Besides, the

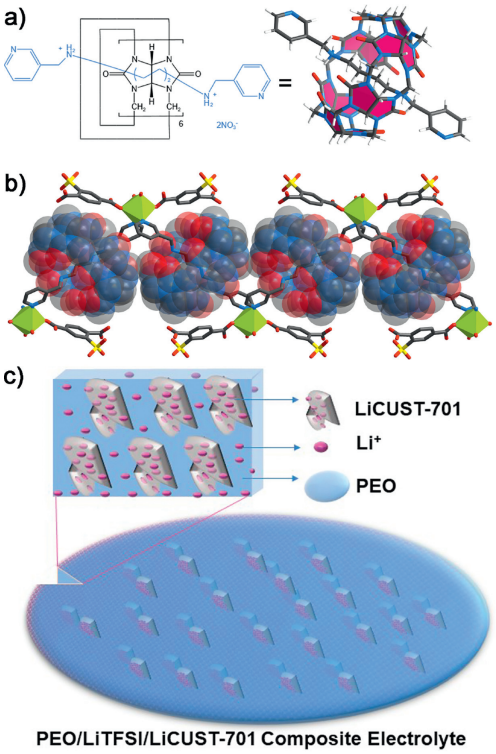

Fig. 1. (a) The chemical structure formula and schematic view of $[PR43]^{2+}\cdot 2[NO_3]^-$. (b) The one-dimensional chain structure diagram of CUST-701. (c) Schematic diagram of PEO/LiTFSI/LiCUST-701 composite electrolyte.

LiCUST-701 was prepared by ion exchange strategy. PXRD and FT-IR show the integrity of frameworks the MORFs was maintained after ion exchange (Figs. S11 and S12 in Supporting information). Inductively coupled plasma atomic emission spectroscopy (ICP) results also illustrate that Li^+ was successfully introduced into the frameworks (Table S3 in Supporting information). The preparation of PEO/LiTFSI/LiCUST-701 complex electrolytes is shown in Fig. 1c and Fig. S1. In order to characterize the effect of solid MOF fillers on the crystallinity of PEO matrix, DSC tests were also performed on pure PEO polymer as well as PEO/0.2LiCUST-701 composites with added solid fillers (Table S7 and Fig S14 in Supporting information). The introduction of MOF solid filler caused the glass transition temperature (T_g) and crystalline melting temperature (T_m) of the PEO matrix to change, as shown in Table S7 the addition of LiCUST-701 transformed the T_m and T_g to −54.96 °C and 58.71 °C. And the corresponding heat enthalpy (ΔH_m) of PEO changes from 156.29 J/g to 62.50 J/g. Crystallinity (χ_c) indicates the relative percentage of crystallinity of the PEO-based polymer electrolyte. The degree of χ_c of the polymer was calculated using the equation in the Supporting Information. The results showed that the added MOF solid fillers significantly reduced the crystallinity of the PEO matrix, which decreased from 77.0% to 30.8%, and the solid fillers were able to improve the ionic conductivity of the composite polymer electrolyte by influencing the chain segment motion of PEO.

In order to explore the ionic conductivity of LiCUST-701 composite electrolyte, the AC impedance of PEO/LiTFSI/LiCUST-701 composite electrolytes with different contents of LiCUST-701 was tested at 25–70 °C in a frequency range of 70–0.1 MHz. As shown in Fig. 2a, the ionic conduction-dominated conduction behavior can be found from the apparent diffusion tail. Fig. 2b and Table S4 (Supporting information) show the conductivities of PEO/LiTFSI/LiCUST-701 composite polymer electrolytes with different LiCUST-701 contents at different temperatures. From the results, we can clearly see that the temperature is positively cor-

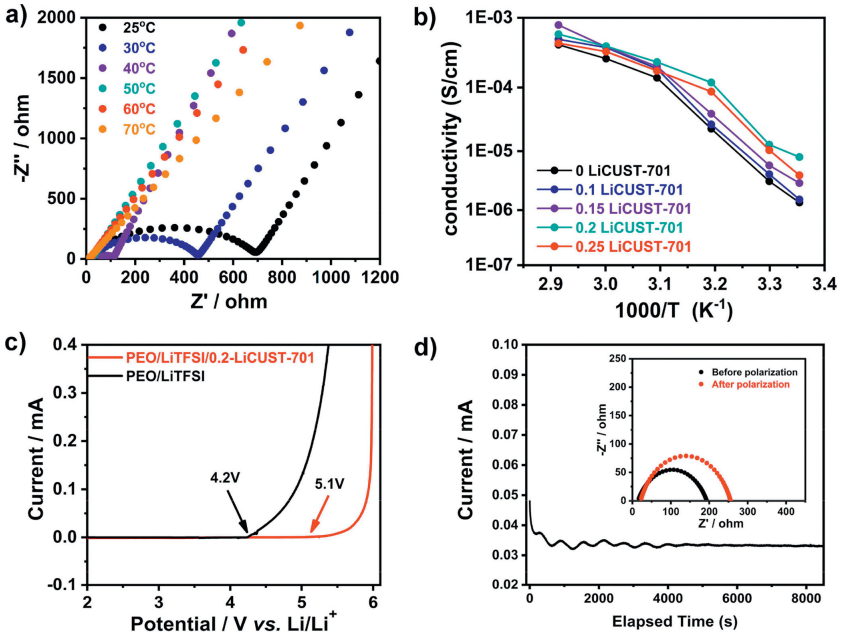

Fig. 2. PEO/LiTFSI/0.2LiCUST-701 composite polymer electrolytes: (a) AC impedance spectra under different temperatures, and (b) conductivity of different doping amounts at different temperatures. (c) LSV curves of Li|PEO/LiTFSI|SS and Li|PEO/LiTFSI/0.2LiCUST-701|SS cells with a scan rate of 1 mV/s at 60 °C. (d) Chronoampere curve of a Li-symmetrical cell at a 10 mV polarization voltage for Li|PEO/LiTFSI/0.2LiCUST-701|Li, the inset is the AC impedance spectrum before and after polarization of the same cell.

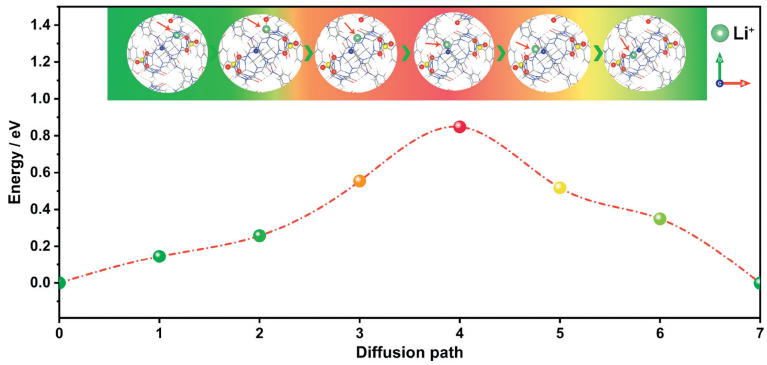

Fig. 3. DFT Calculations. Possible diffusion paths for lithium ions in **CUST-701**.

related with the conductivity. As the doping amount of LiCUST-701 gradually increased from 0 to 15%, their conductivities also gradually increased from 4.23×10^{-4} S/cm to 0.795×10^{-3} S/cm (70 °C). The conductivity of PEO/LiTFSI/0.2LiCUST-701 is the highest at different temperatures. The exception is that the conductivity of PEO/LiTFSI/0.15LiCUST-701 is relatively the highest at 70 °C. We speculate that with the increase of temperature to 70 °C, the movement of PEO chain segment is intense, and the slightly excessive filler may have a negative effect on the Li^+ conduction to some extent, leading to a decrease in conductivity. When the doping amount increases to 25%, the conductivity decreases throughout the temperature range due to a fact that the excessive amounts of LiCUST-701 particles tend to agglomerate. The E_a values for PEO/LiTFSI/0.2LiCUST-701 are 1.27 eV and 0.47 eV in the two temperature ranges, which are lower than the E_a values of PEO/LiTFSI at the corresponding conditions (1.57 eV and 0.54 eV) (Table S5 in Supporting information). Bonding energies of lithium ions at potential adsorption sites in CUST-701 structures were described by DFT calculations, as shown in Table S6 (Supporting information), the sulfonic acid moiety is the most promising adsorption site. The possible transfer paths of lithium ions in CUST-701 are visualized through theoretical calculations (Fig. 3). The lithium ion binding to the sulfonate oxygen atom first transferred to the nearby positions of the CB[6] carbonyl oxygen atom. After that Li^+ pass by to the nitrogen atom of the ring, and then the lithium ion transferred to the oxygen atom of another adjacent sulfonic acid group.

The strain–stress curves of PEO/LiTFSI, PEO/LiTFSI/0.2LiCUST-701 electrolyte films have been measured to investigate the mechanical performances of the composite electrolyte membranes. As shown in Fig. S13 (Supporting information), both film samples tested underwent a softening process, and then their stresses reached the maximum values. This is followed by the quasi-plateau region with high plastic strain of films. The cracking and stress rupture of PEO/LiTFSI films occur when the strain increases to 270%. In comparison, PEO/LiTFSI/0.2LiCUST-701 film can withstand more than 375% of strain. Meanwhile, the maximum stress of PEO/LiTFSI film is 2.5 MPa, which is higher than that of PEO/LiTFSI/0.2LiCUST-701 film (1.7 MPa). The strain-stress test indicates the incorporating of LiCUST-701 into PEO polymer matrix can effectively improve the pliability of the composite electrolyte films.

The oxidation potential of the electrolyte has an important impact on the application of the electrolyte. The electrochemical stability of Li|SSE|SS half-cell at high voltage has been investigated by linear scanning voltammetry (LSV) at 60 °C (Fig. 2c). The PEO/LiTFSI/0.2LiCUST-701 composite electrolyte can achieve an oxidative stability of 5.1 V. In contrast, the PEO/LiTFSI electrolyte

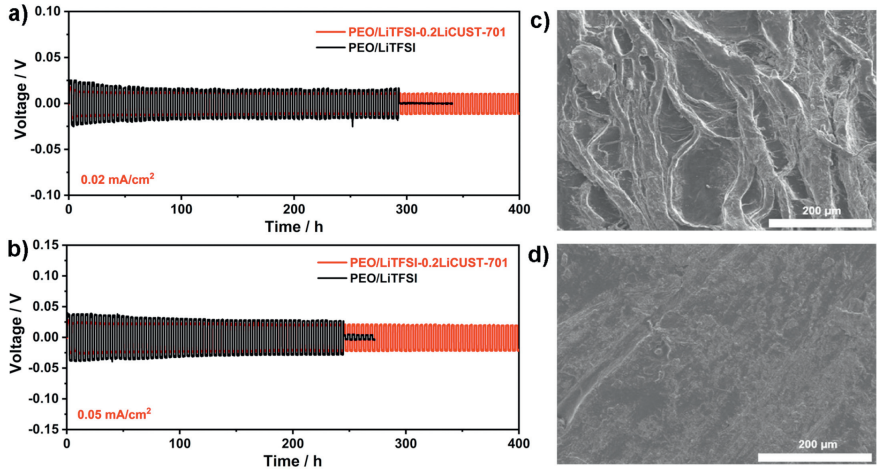

Fig. 4. Voltage-time distribution curves for Li|PEO/LiTFSI|Li and Li|PEO/LiTFSI/0.2LiCUST-701|Li symmetric cells at (a) 0.02 mA/cm^2 and (b) 0.05 mA/cm^2. SEM images of symmetric cells after cycling of lithium sheets (all at 60 °C) for (c) Li|PEO/LiTFSI|Li and (d) Li|PEO/LiTFSI/0.2LiCUST-701|Li.

oxidation occurs at around 4.2 V. In general, the lithium-ion migration number can evaluate the ion transport capacity of the electrolyte. The PEO/LiTFSI and PEO/LiTFSI/0.2LiCUST-701 composite electrolytes were subjected to chronoamperometric tests (Fig. 2d). The results suggest that PEO/LiTFSI had a t_+ value of 0.15, while the PEO/LiTFSI/0.2LiCUST-701 composite polymer electrolyte had a t_+ value of 0.46. This may be due to the sulfonic acid groups of frameworks after ion exchange is able to dissociate Li^+, while the electropositive outer surface of CB[6]s molecule is likely to interact electrostatically with $TFSI^-$, thus limiting the movement of $TFSI^-$ and promoting the dissociation and transfer of Li^+ [29–32]. Compared with the reports in the last two years about PEO-based solid electrolytes using MOFs as solid fillers (Table S8), it achieves a better overall performance and employs a novel strategy of introducing supramolecular macrocycles. At the same time, the decomposition of LiTFSI ion pair promotes local relaxation and segmentation of polymer, which generates more free Li^+ and further improves the electrochemical stability of electrolyte at high voltage.

The lithium plating/exfoliation behavior and cycling stability have been also investigated by constant current discharge/charge voltage curves. As shown in Fig. 4a, the polarization voltage of the Li|PEO/LiTFSI/0.2LiCUST-701|Li cell is 10 mV at a current density of 0.02 mA/cm^2, while the polarization voltage of Li|PEO/LiTFSI|Li cell is 15 mV and a short-circuit voltage occurs after about cycling of 290 h, the circuit voltage drops to 0 V. In comparison, the Li|PEO/LiTFSI/0.2LiCUST-701|Li cell exhibits a stable voltage plateau over 400 h. Fig. 4b shows the voltage-time distribution curves at polarization voltage of 10 mV and a current density of 0.05 mA/cm^2, Li|PEO/LiTFSI|Li cell also showed a sudden voltage drop after 240 h, while the Li|PEO/LiTFSI/0.2LiCUST-701|Li cell still could keep stable for over 400 h. After the cycling of the cell constructed with polymer electrolytes, the surface morphology of lithium metal sheets has been observed and compared. A large amount of lithium dendrites was produced on the surface of the lithium sheets after cycling (Fig. 4c). In contrast, the lithium sheets of Li|PEO/LiTFSI/0.2LiCUST-701|Li cell present relatively smooth and dense morphology with almost no dendrites on the surface after cycling (Fig. 4d). This is in line with the improved cell cycling stability, which indicates the inhibited lithium dendrite growth of composite polymer electrolyte is due to uniform deposition of lithium metal induced by its high Li^+ migration. At the same time, the good mechanical properties of the composite electrolyte film can mitigate the short circuit hazard caused by lithium dendrite growth [12,33].

The CR2025 type full cell was assembled with $LiFePO_4$ as the cathode material and lithium metal foil as the negative electrode. The constant current charging and discharging of full cells was measured at 60 °C in the voltage range of 2.5–4.2 V. Fig. 5a shows the cycling performance of Li|PEO/LiTFSI|$LiFePO_4$ and Li|PEO/LiTFSI/0.2LiCUST-701|$LiFePO_4$ cells at 0.2 C. The Li|PEO/LiTFSI|$LiFePO_4$ cell had fast capacity decay and low coulomb efficiency. The first discharge capacity after activation was 116 mAh/g and after 100 cycles the capacity was 52 mAh/g, which was only 44.8% of the initial capacity. In contrast, the Li|PEO/LiTFSI/0.2LiCUST-701|$LiFePO_4$ cell exhibited a gentle discharge curve with a capacity of 148 mAh/g at the first discharge and 134 mAh/g (a 90.5% capacity retention) after 100 cycles. Meanwhile, the coulomb efficiency rate was almost close to 100%. Comparing the multiplicity performance of the two cells (Fig. 5b), the capacities of Li|PEO/LiTFSI|$LiFePO_4$ cell at 0.1, 0.2, 0.5, 1 and 2 C current rates were 131, 115, 100, 73 and 41 mAh/g, respectively. Li|PEO/LiTFSI/0.2LiCUST-701|$LiFePO_4$ cell exhibited higher capacity with capacities of 150, 144, 131, 117, and 98 mAh/g at different current rates of 0.1, 0.2, 0.5, 1, and 2 C, respectively. And Li|PEO/LiTFSI/0.2LiCUST-701|$LiFePO_4$ had excellent capacity recovery from 98 mAh/g to 145 mAh/g with the current density changing from 2 C to 0.1 C, which essentially matched with its initial capacity. Then, the cycling capability of the Li|PEO/LiTFSI/0.2LiCUST-701|$LiFePO_4$ cell with high current density has been investigated, which showed a first discharge capacity of 124 mAh/g at 2 C and a stable discharge capacity of 103 mAh/g (an 83% capacity retention) after 270 charge/discharge cycles (Fig. 5c). Meanwhile, the coulomb efficiency was close to 100%. The addition of LiCUST-701 could effectively inhibit the growth of lithium dendrites and improve the cycling stability of solid-state batteries.

In summary, a new MORF (CUST-701) was successfully synthesized *via* combining of Zn^{2+}, [PR43]s and 2-H_2stps (2-sulfoterephthalic acid monosodium salt) in hydrothermal methods. By using ion-exchange strategy, CUST-701 was modified by Li^+ to obtain LiCUST-701. And the transfer path of lithium ions in LiCUST-701 was speculated through DFT calculations. Subsequently, the composite electrolytes were constructed by incorporating LiCUST-701 into PEO matrix. The experimental results showed that the incorporation of LiCUST-701 could enhance the pliability of the polymer electrolytes and mitigate the effect of lithium dendrites on the battery lifetime, which is a key factor affecting the performance of solid-state batteries. The sulfonic acid groups located in the MORF and positively charged outer surface of CB[6]s can interact with the $TFSI^-$, which promoted the dissociation of LiTFSI

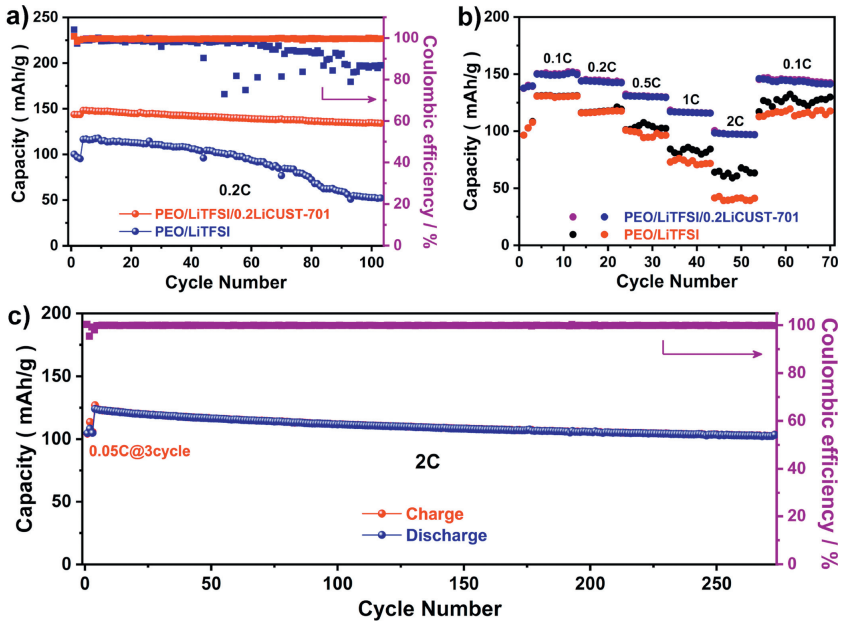

Fig. 5. Li|PEO/LiTFSI|$LiFePO_4$ and Li|PEO/LiTFSI/0.2LiCUST-701|$LiFePO_4$ cells: (a) Cycling performance at 0.2 C, and (b) multiplicity performance. (c) Cycling performance Li|PEO/LiTFSI/0.2LiCUST-701|$LiFePO_4$ cells at 2 C (All the above tests were performed at 60 °C).

ion pairs, increased the Li^+ content and thus improved the conductivities and Li^+ migration number of the polymer electrolyte. The all-solid-state lithium-metal batteries assembled with composite polymer possess high discharge capability and excellent cycling stability even after long cycles at high current densities. We anticipate that more CB[6]-based solid-state composite electrolytes with high lithium ion conductivities would be designed and constructed by this effective strategy in the future.

Declaration of competing interest

The authors declare that they have no known competing financial interests or personal relationships that could have appeared to influence the work reported in this paper.

Acknowledgments

The authors gratefully acknowledge the financial support from the National Natural Science Foundation of China (Nos. U1973201 and 22271023).

Supplementary materials

Supplementary material associated with this article can be found, in the online version, at doi:10.1016/j.cclet.2023.109189.

References

[1] Y. Chen, K. Wen, T. Chen, et al., Energy Storage Mater. 31 (2020) 401–433.
[2] J. Duan, W. Wu, A.M. Nolan, et al., Adv. Mater. 31 (2019) 1807243.
[3] Z. Zhang, Y. Huang, H. Gao, et al., J. Energy Chem. 60 (2021) 259–271.
[4] C. Sun, J. Zhang, X. Yuan, et al., ACS Appl. Mater. Interfaces 11 (2019) 46671–46677.
[5] A.E. Abdelmaoula, J. Shu, Y. Cheng, et al., Small Methods 5 (2021) 2100508.
[6] X. Lu, H. Wu, D. Kong, et al., ACS Mater. Lett. 2 (2020) 1435–1441.
[7] D.M. Shin, J.E. Bachman, M.K. Taylor, et al., Adv. Mater. 32 (2020) 1905771.
[8] J. Janek, W.G. Zeier, Nat. Energy 1 (2016) 16141.
[9] T. Wei, Z. Wang, Q. Zhang, et al., CrystEngComm 24 (2022) 5014.
[10] X. Liu, X. Li, H. Lia, et al., Chem. Eur. J. 24 (2018) 18293–18306.
[11] D.E. Mathew, S. Gopi, M. Kathiresan, et al., Electrochim. Acta 319 (2019) 189–200.
[12] L. Yue, J. Ma, J. Zhang, et al., Energy Storage Mater. 5 (2016) 139–164.
[13] G. Lu, H. Wei, C. Shen, et al., ACS Appl. Mater. Interfaces 14 (2022) 45476–45483.
[14] Y. Hu, X. Xie, W. Li, et al., ACS Sustain. Chem. Eng. 11 (2023) 1253–1277.
[15] L. Sun, S.S. Park, D. Sheberla, et al., J. Am. Chem. Soc. 138 (2016) 14772–14782.
[16] W. Xu, X. Pei, C.S. Diercks, et al., J. Am. Chem. Soc. 141 (2019) 17522–17526.
[17] Y. Qian, Z. Liu, H. Song, et al., Chin. Chem. Lett. 35 (2024) 108785.
[18] X. Wu, K. Chen, Z. Yao, et al., J. Power Sources 501 (2021) 229946.
[19] S. Fischer, J. Roeser, T.C. Lin, et al., Angew. Chem. Int. Ed. 57 (2018) 16683–16687.
[20] Z. Wang, H. Zhou, C. Meng, et al., ACS Appl. Energy Mater. 3 (2020) 4265–4274.
[21] J. Wan, J. Xie, D.G. Mackanic, et al., Mater. Today Nano 57 (2018) 1–16.
[22] W. Yang, H.J. Wang, R.R. Liu, et al., Angew. Chem. Int. Ed. 60 (2021) 409.
[23] D.C. Zhong, Y.N. Gong, C. Zhang, et al., Chem. Soc. Rev. 52 (2023) 3170–3214.
[24] S. Jiang, T. Lv, Y. Peng, et al., Adv. Sci. 10 (2023) 2206887.
[25] Z. Zhang, L. Tian, H. Zhang, et al., ACS Appl. Energy Mater. 5 (2022) 1095–1105.
[26] C. Li, S. Deng, W. Feng, et al., Small 19 (2023) 2300066.
[27] X.L. Ni, X. Xiao, H. Cong, et al., Acc. Chem. Res. 47 (2014) 1386–1395.
[28] F. Zhang, T. Yajima, Y.Z. Li, et al., Angew. Chem. Int. Ed. 44 (2005) 3402–3407.
[29] X.L. Ni, X. Xiao, H. Cong, et al., Chem. Soc. Rev. 42 (2013) 9480–9508.
[30] G.G. Eshetu, X. Judez, C. Li, et al., J. Am. Chem. Soc. 140 (2018) 9921–9933.
[31] Y. Xu, S. Zhang, T. Liang, et al., ACS Appl. Mater. Interfaces 13 (2021) 11018–11025.
[32] Z. Zou, Y. Li, Z. Lu, et al., Chem. Rev. 120 (2020) 4169–4221.
[33] F. Ye, K. Liao, R. Ran, et al., Energy Fuels 34 (2020) 9189–9207.